



**HAL**  
open science

# Intraspherulitic mechanical heterogeneities and microstructure of i-PP highlighted by nanoindentation and atomic force microscopy

Jérémy Grondin, Olga Smerdova, Sylvie Castagnet, Christophe Tromas

## ► To cite this version:

Jérémy Grondin, Olga Smerdova, Sylvie Castagnet, Christophe Tromas. Intraspherulitic mechanical heterogeneities and microstructure of i-PP highlighted by nanoindentation and atomic force microscopy. *Polymer*, 2023, 285, pp.126391. 10.1016/j.polymer.2023.126391 . hal-04299326

**HAL Id: hal-04299326**

**<https://hal.science/hal-04299326>**

Submitted on 22 Nov 2023

**HAL** is a multi-disciplinary open access archive for the deposit and dissemination of scientific research documents, whether they are published or not. The documents may come from teaching and research institutions in France or abroad, or from public or private research centers.

L'archive ouverte pluridisciplinaire **HAL**, est destinée au dépôt et à la diffusion de documents scientifiques de niveau recherche, publiés ou non, émanant des établissements d'enseignement et de recherche français ou étrangers, des laboratoires publics ou privés.

CRediT

# Intraspherulitic mechanical heterogeneities and microstructure of *i*-PP highlighted by Nanoindentation and Atomic Force Microscopy

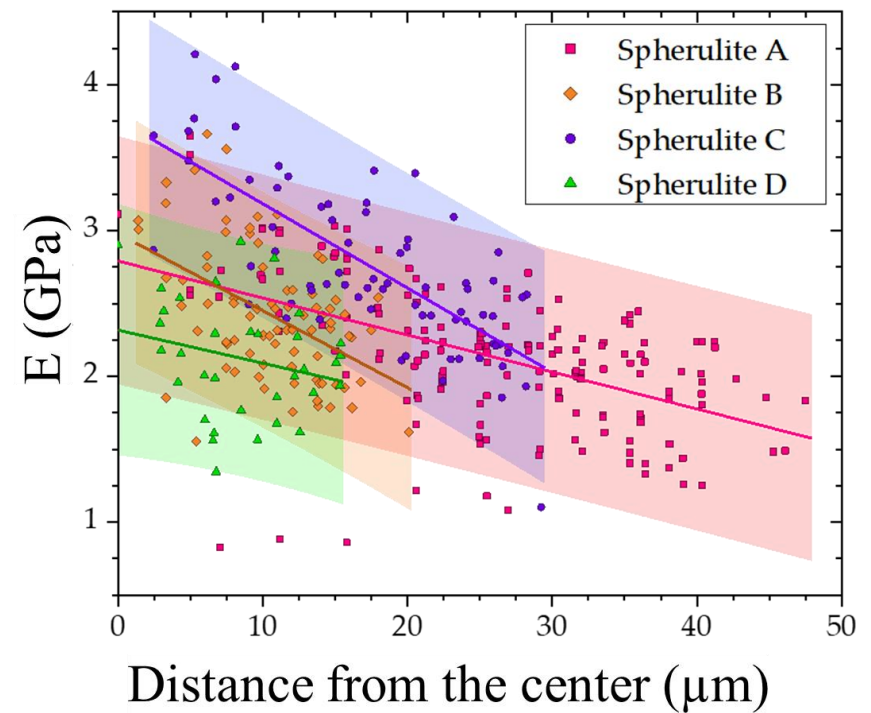
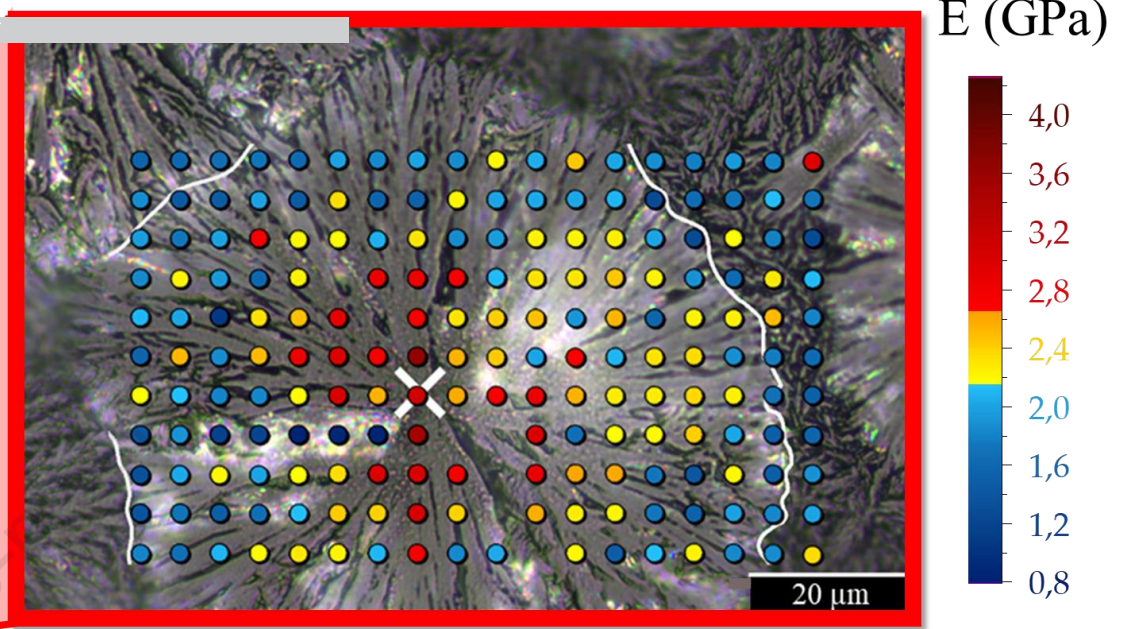
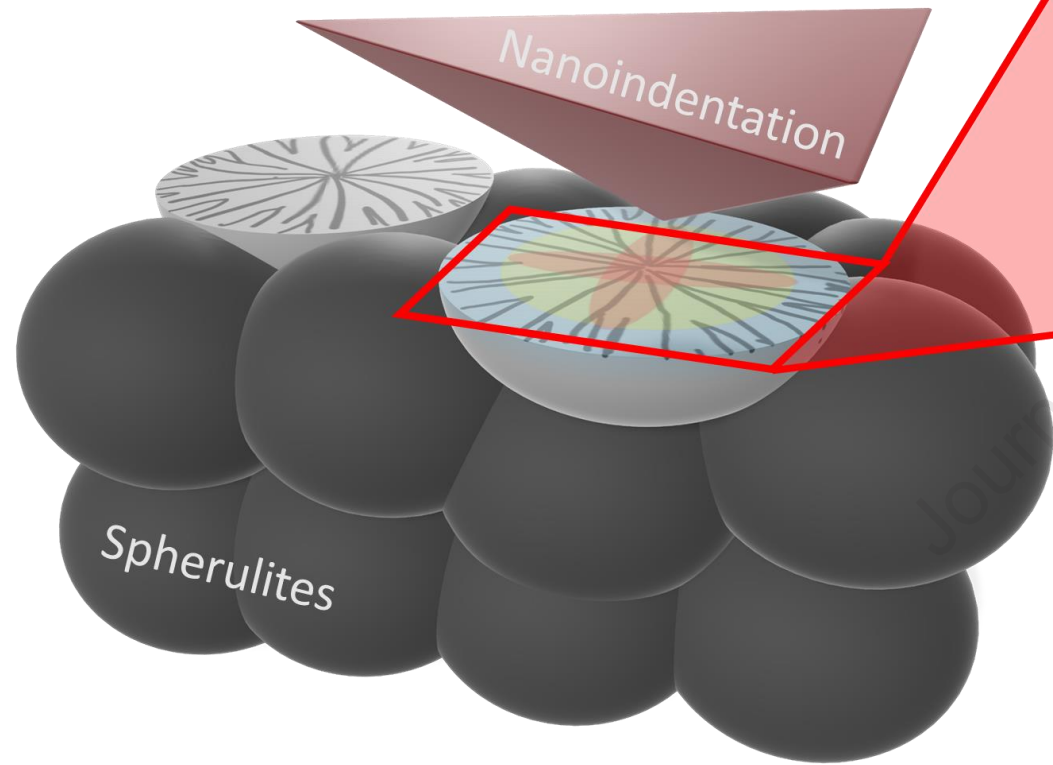
Jérémy GRONDIN\*<sup>1</sup>, Olga SMERDOVA<sup>1</sup>, Sylvie CASTAGNET<sup>1</sup>, Christophe TROMAS<sup>1</sup>

<sup>1</sup>Institut Pprime (UPR 3346 CNRS / ISAE-ENSMA / UNIVERSITÉ DE POITIERS), Department of Physics and Mechanics of Materials, 1 Avenue Clement Ader, BP 40109, Futuroscope, 86961, Cedex, France

\*Corresponding author.

Email address: [jeremy.grondin@ensma.fr](mailto:jeremy.grondin@ensma.fr) (J. Grondin)

**Jérémy Grondin:** Investigation, Formal analysis, Data Curation, Writing - Original Draft, Conceptualization, Methodology, Visualization, Validation. **Olga Smerdova:** Conceptualization, Funding acquisition, Writing - Review & Editing, Validation, Project administration, Supervision. **Sylvie Castagnet:** Conceptualization, Writing - Review & Editing, Validation, Supervision. **Christophe Tromas:** Conceptualization, Methodology, Writing - Review & Editing, Validation, Supervision.



# Intraspherulitic mechanical heterogeneities and microstructure of *i*-PP highlighted by Nanoindentation and Atomic Force Microscopy

5 Jérémy GRONDIN\*<sup>1</sup>, Olga SMERDOVA<sup>1</sup>, Sylvie CASTAGNET<sup>1</sup>, Christophe TROMAS<sup>1</sup>

<sup>1</sup>Institut Pprime (UPR 3346 CNRS / ISAE-ENSMA / UNIVERSITÉ DE POITIERS),  
Department of Physics and Mechanics of Materials, 1 Avenue Clement Ader, BP 40109,  
Futuroscope, 86961, Cedex, France

10

\*Corresponding author.

Email address: [jeremy.grondin@ensma.fr](mailto:jeremy.grondin@ensma.fr) (J. Grondin)

## Abstract

15

This study quantifies elastic modulus heterogeneity at the intraspherulitic scale in semi-crystalline *i*-PP polymer using nanoindentation. Prior to mechanical characterization, Atomic Force Microscopy (AFM) is used to characterize the topography of the local micro- and nanostructure of the spherulites. Small indents provide 3-5  $\mu\text{m}$  resolution maps within a spherulite, remaining unaffected by local roughness. The major findings highlight a clear relationship between microstructure and mechanical properties at this scale. Firstly, elastic modulus decreases from the spherulite center to the edges. Secondly, regions along the main growth axes exhibit higher modulus values, while areas around these axes are less stiff.

Moreover, similar elastic properties are found at the ends of spherulite branches measured in a  
25 transverse and longitudinal orientation with respect to the growth axis. The difference in  
measured mechanical properties is attributed to the local density and orientation of crystalline  
lamellae, which in turn depend on the spherulite's growth stage.

## Keywords

30 Semi-crystalline polymers ; nanoindentation ; AFM

## 1 Introduction

The relationships between microstructure and mechanical properties are still of huge interest  
35 for the improvement of semi-crystalline polymer performance and for the optimization of  
forming processes. Due to their complex and multi-scale organization, such relationships are  
still only partially elucidated. In semi-crystalline polymers classically crystallized from the  
melt, the macroscopic mechanical properties are defined by several scale transitions, from the  
molecular level through the elementary amorphous/crystalline lamellar stacks and up to the  
40 extraordinarily complex spherulitic mesoscale made of lamellae ramifications. The role of each  
scale is not fully understood and is limited by two main challenges. The first difficulty is to  
capture the microstructure, especially at fine scales considering the weak electronic density  
contrast of phases, which limits the use of X-ray-based techniques. The second one is to access  
the mechanical properties over a wide scale range due to a lack of experimental techniques  
45 operating directly at small scales.

From the beginning, the lamellar scale has been mostly investigated, and often empirically connected to the macroscopic scale without consideration of intermediate mesoscopic structure. Historically, direct relationships have been established, like those between the global crystallinity ratio or the average crystalline lamellae thickness with the elastic modulus or the tensile yield stress of macroscopic samples, especially for PE [1–4]. More recently, analyses from in-situ small and wide-angle X-ray scattering (SAXS / WAXS) experiments helped researchers better quantify the local kinematics at the lamellar scale and refined the understanding of the lamellar microstructure influence on these mechanical parameters [5–9]. However, the local mechanical properties were usually deduced from the reverse analysis of one-dimensional average lamellar stack modeling, resulting in a simplified local strain field. Furthermore, advancements in Atomic Force Microscopy (AFM) using mechanical mode have led to numerous efforts over the past decade to assess localized mechanical properties, including the elastic modulus, on the scale of crystalline lamellae [10–12]. However, it is worth noting that the morphologies typically studied in these cases are not commonly associated with spherulitic structures. It is also important to consider that these techniques have not yet achieved robust quantitative validation. This is partly due to the challenge of precisely characterizing the tip shape, a critical input in the interpretation models.

The status and role of the spherulitic scale in the scale transition are still unclear and very often omitted from the mechanical analyses. However, it appears that the spherulitic microstructure, as well as the deformation and damage mechanism, have been much better characterized over the last 20 years.

For instance, some authors studied the plasticity and damage mechanisms of the microstructure by doing monotonic tensile tests on semi-crystalline polymer films and making ex-situ [13,14] or in-situ [15,16] observations by AFM. Studies involving spherulitic deformation mechanisms for thick samples can also be found, either using scanning electron microscopy (SEM)

observations [17] or tomographic techniques [18,19]. These studies generally give qualitative information on spherulitic deformation, such as plastic or damage mechanisms, without giving quantitative properties at the microstructure scale. Only a few authors have tried to give quantitative information on the kinematics, e.g., using in-situ Digital Image Correlation (DIC) in SEM to assess the strain field at the spherulitic scale in the case of a monotonic tensile test [20]. However, the measurement of the stress field did not fully clarify the local mechanical properties. Moreover, many studies have focused on thin films or polymers in solution [21], leading to rather artificial two-dimensional spherulites.

In this context, nanoindentation is an interesting technique to quantify the mechanical behavior of such multiscale material. This technique consists in penetrating a tip of known geometry into the surface of the material. Thanks to the force-displacement curve, it is then possible to determine the mechanical properties of the material (indentation elastic modulus and hardness) through a simple analytic model. Although these measurements are performed in an elasto-plastic framework, which is restrictive for polymers exhibiting time-related behavior, it is a convenient test to obtain mechanical properties at small scales. Nanoindentation is most often used for the characterization of polymers considered homogeneous such as amorphous polymers like PMMA [22–25], PC [24,26], or PS [24]. For semi-crystalline polymers, nanoindentation was used on commercial samples prepared by conventional manufacturing processes, such as injection molding or extrusion, that usually induce a microstructure gradient between the skin and the core of the sample [27–33]. These studies aimed to evaluate the mechanical response in the different zones (skin-transition-core layers) of the prepared sample. It should be noted that although these studies attempt to establish links between local crystallinity and mechanical response, the contribution of the spherulitic microstructure to this response is not clearly addressed, and it is not possible to obtain highly localized crystallinity of the material. Labour *et al.* [34] are one of the first to have used nanoindentation to investigate

the mechanical properties of semi-crystalline isotactic polypropylene (*i*-PP) at the spherulitic scale and to draw direct links between spherulite type and its mechanical response. The depth of indentation was fixed to 500 nm giving the equivalent contact diameter of 3.5  $\mu\text{m}$ . This tested volume was too high to obtain a fine mechanical characterization of the heterogeneities inside a spherulite and only average tendencies were obtained. The authors found that the elastic modulus and hardness of  $\beta$ -spherulites were respectively 10% and 15% lower on average than those of  $\alpha$ -spherulites. This difference is similar whether the surface has been annealed after polishing or chemically etched after polishing.

A study by Enrique-Jimenez et al. [35] on a semi-crystalline poly(3-hydroxybutyrate-co-3-hydroxyvalerate) copolymer film focused on the distribution of the mechanical properties within a banded spherulite measured by nanoindentation. This study revealed that the elastic modulus and hardness distribution across the banding morphology exhibits a series of regular oscillations, with a periodicity that matches the pattern observed under both optical and atomic force microscopy. However, the possible influence of the topography of such ring-banded spherulites on the results of nanoindentation can be questioned and no observation of the residual indents was performed to shed light on this issue. Indeed, one of the limitations of using nanoindentation is the need for a flat and smooth surface. Thus, most of the cited authors polish surfaces to ensure their suitability for nanoindentation [27,28,33,34,36,37]. However, polishing erases a layer of material and partially destroys the microstructure. It has been shown that polishing induces a hardening of the surface of PEEK polymer leading to an overestimation of up to 10% of the hardness for low indentation depths (<200 nm)[33].

Given the lack of knowledge on the intraspherulitic mechanical heterogeneities, the *i*-PP polymer was selected in this study for its ability to grow large spherulites, as a first-ever attempt to obtain and relate the mechanical properties at several scales from nanometric to macrometric on the same microstructure. This paper, which is part of a larger multiscale study, aims at the

mechanical characterization of the heterogeneities inside spherulitic branches of different sizes and orientations. The sample preparation protocol was deliberately chosen to obtain three-dimensional freely grown spherulites without destruction of the surface layer by polishing. The nanoindentation technique was used to provide maps of the elastic modulus within several more or less developed spherulites nucleated either in the volume or close to the surface. Optical microscopy and AFM scans were used to thoroughly study the spherulite morphology and topography and validate nanoindentation results.

## 2 Material and Methods

130

A thick sample (1.5 mm) of *i*-PP was prepared from pellets purchased from a commercial supplier (GoodFellow, UK; product code PP306315). A circular cavity ( $\varnothing 20 \times 1.5$  mm) of a textured steel mold was filled with the pellets, and the mold was placed in an oven at 220°C for 25 minutes. Then, the mold was taken out of the oven and cooled at room temperature. The sample was then progressively polished with diamond polishing suspensions (3  $\mu\text{m}$  grains for 45 minutes and 1  $\mu\text{m}$  grains for 15 minutes) to obtain the flat surface required for nanoindentation experiments and finally melted again at 190°C for 30 minutes to create a new spherulitic microstructure at the surface.

135

Differential scanning calorimetry (DSC) and wide-angle X-ray scattering (WAXS) were used to investigate the thermal and microstructural properties of the *i*-PP material. DSC measurements were performed on a sample subjected to the same heating treatment as the one used for the nanoindentation testing using a *TA Instruments Q20* at a heating rate of 10°C/min from 25°C to 250°C in an air atmosphere. The resulting DSC data, presented in Fig. 1, revealed a crystallization temperature ( $T_c$ ) and a melting temperature ( $T_m$ ) of 109°C and 166°C

140

145 respectively, characteristic of the  $\alpha$  phase of *i*-PP [38]. The degree of crystallinity was determined using the enthalpy of fusion method, with a theoretical enthalpy of 165 J/g for 100% crystalline  $\alpha$ -phase *i*-PP [39]. The calculated degree of crystallinity was 50%. The WAXS measurements were conducted on another sample obtained from the same original pellets using a *Bruker D8 Discover* diffractometer with a copper  $K\alpha_1$ - $K\alpha_2$  radiation source ( $\lambda = 1.54060$ ,  
150 1.54439 Å) at  $2\theta$  angles of  $8^\circ$  to  $60^\circ$  for 200 seconds. The WAXS data (cf. Electronic Supplementary Information) revealed peaks characteristic of the  $\alpha$  phase of *i*-PP, which is consistent with the results obtained from the DSC experiment despite different thermal history of the samples. Indeed DSC comparative test (cf. Electronic Supplementary Information) was conducted between the original *i*-PP pellets and a sample that followed exactly the same thermal  
155 protocol as the one tested by nanoindentation, revealing high similarity in melting and crystallization peaks.

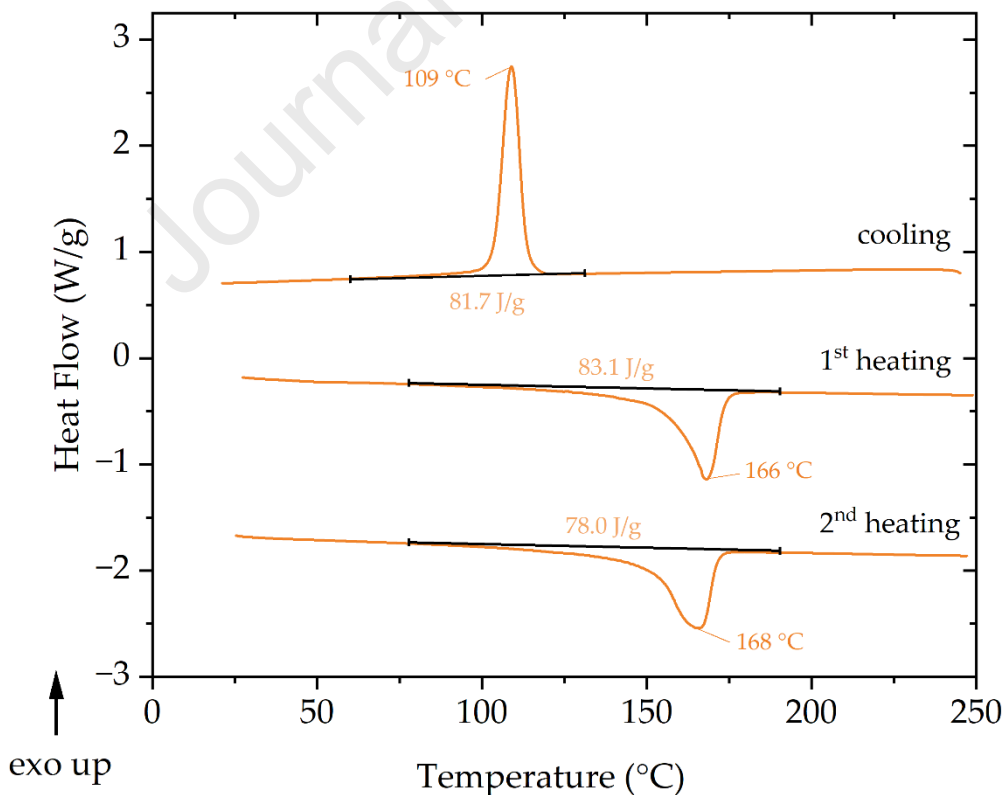


**Fig. 1 - DSC curves obtained from a sample subjected to the same heating treatment as the one used for the nanoindentation testing.**

A first morphological characterization of the surface microstructure was done by optical microscopy using a *Brucker Alicona Infinite Focus* optical microscope. Then, surface topography was characterized at the nanometer scale by Atomic Force Microscopy (*Brucker Dimension Icon*) operated in *PeakForce Tapping*® mode.

The mechanical properties at the intraspherulitic scale of the material were determined by nanoindentation (*UNHT, Anton Paar*) using a Berkovich diamond tip. The tip area function has been rigorously calibrated on fused silica [40]. The results presented in this paper are focused on the elastic properties. The hardness values obtained simultaneously in the analysis are provided in Electronic Supplementary Information.

Four indentation arrays were performed at room temperature on the surface using depth-controlled loading and load-controlled unloading (cf. **Fig. 2**). For the first array, the maximum indentation depth was 200 nm and the step size was 5  $\mu\text{m}$  for a grid of  $18 \times 11$  indents. To improve spatial resolution, the other three tests were performed at a maximum indentation depth of 180 nm and a step size of 3  $\mu\text{m}$ . Their grids are formed by  $12 \times 13$  indents,  $13 \times 9$  indents, and  $14 \times 8$  indents. The loading phase was displacement-controlled and lasted 60 s for the first array (**Fig. 2**) and 30 s for the others, followed by a 30-s displacement-controlled holding period. The unloading phase was then load-controlled and lasted 10 s. These long holding times followed by a short unloading time were chosen to minimize the viscoelastic effects during unloading [26]. Thus, assuming that the beginning of the unloading curve consists of elastic recovery of the material, the indentation modulus was calculated from the fitted unloading curve using the Oliver-Pharr analysis method [40]. This analysis requires the value of Poisson's ratio of the material which was assumed to be constant and equal to  $\nu = 0.38$  [41]. It is worth mentioning that the calculation of the indentation modulus is not highly sensitive to the variation of this parameter (e.g., using  $\nu = 0.30$  instead of  $\nu = 0.38$  would only result in a variation of 5.5%). Furthermore, choosing a single value for  $\nu$  makes sense here because the investigated scale

remains much larger than the scale of the crystalline/amorphous phases, which may have different elastic properties, themselves.

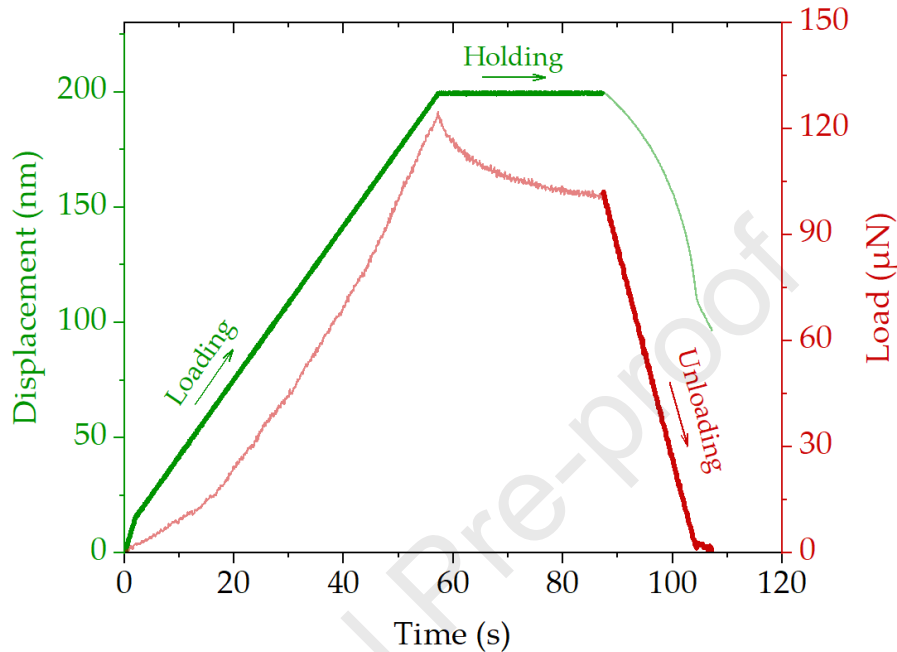


*Fig. 2 - Typical Load-Hold-Unload cycle used for the nanoindentation tests. Note displacement control on loading and holding phases and load control on unloading phase.*

## 185 3 Results and Discussions

### 3.1 Characterization of the surface morphology by Optical Microscopy

**Fig. 3** shows the optical microscopy image captured using non-polarized reflected light, of the sample surface. It is reminded that no chemical treatment was used to reveal the microstructure.

190 Spherulites are easily distinguishable, with an average diameter of about a few tens of microns. As imaged at the surface, they are observed from two different points of view. On one hand, some spherulites were nucleated very closely to the surface. They grew in the surface plane and

through the bulk, leading to a likely hemispheric final shape. Such a situation allows to investigate what could be regarded as a medium plane of the spherulite, with radial branches.

195 On the other hand, the other spherulites were nucleated deeper below the surface. Surface observation reveals their external periphery, as a collection of rather randomly organized objects. As detailed later from AFM observations, their size matches with the extremity of branches observed when nucleation occurred near the surface. **Fig. 4** provides a schematic representation of these two situations.

200 Among the spherulites nucleated near the surface, different sizes and shapes can be observed. Firstly, it could depend on their growth completion. Spherulites that had time and space to crystallize appear as quasi-circular at the surface whereas those whose growth was stopped earlier exhibit a more oblong sheaf-like shape. The former ones are not that much observed, due to the fast-cooling rate occurring at the surface. Secondly, Olley and Basset [42] showed  
205 that the appearance of *i*-PP spherulite could strongly depend on orientation. In the early or intermediate stages of growth, they evidenced that the  $\alpha$ -form spherulites could appear either sheaf-like (two lobes) or rosette-shaped (four lobes) depending on the considered angle of view.

Still regarding spherulites nucleated near the surface, some shiny areas are visible on the optical microscopy image in **Fig. 3**. They are mainly located on the sides of the growth axes of the  
210 spherulites and sometimes at the extremities of the branches. This brightness effect reflects different optical properties of the spherulites depending on the considered zone. Possible causes will be discussed later in **section 3.3**.

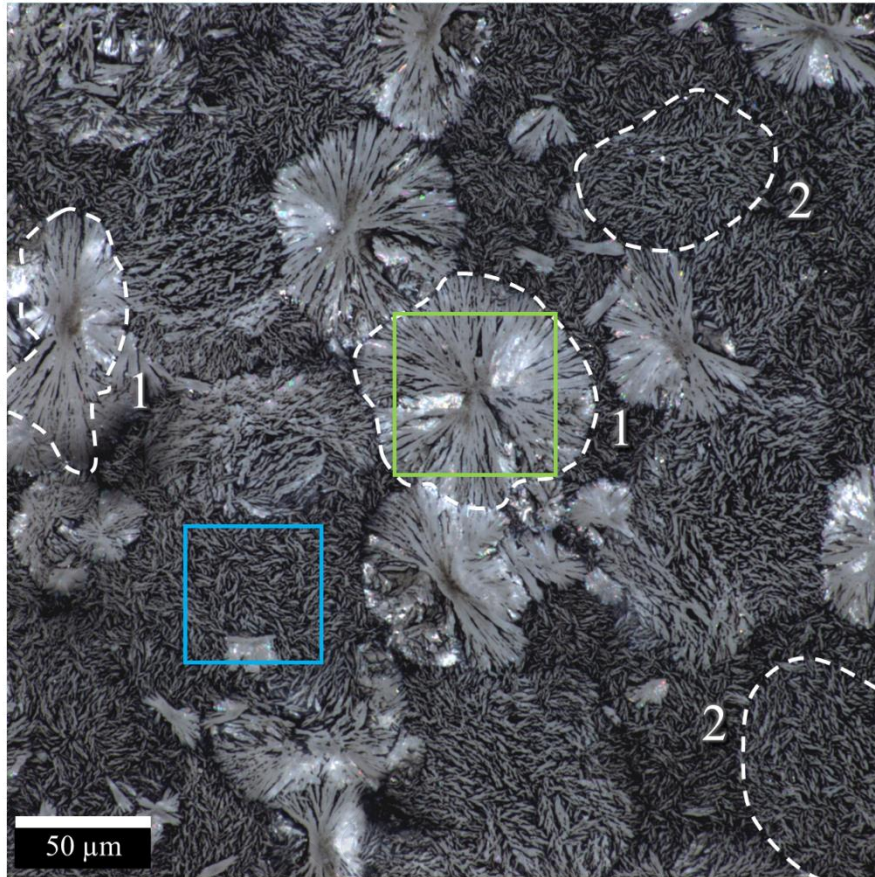


Fig. 3 - Surface of the thick sample observed by optical microscopy with **non-polarized reflected light**. Examples of spherulites nucleated near the surface (labeled as 1) and deeper in the volume (labeled as 2) are highlighted.

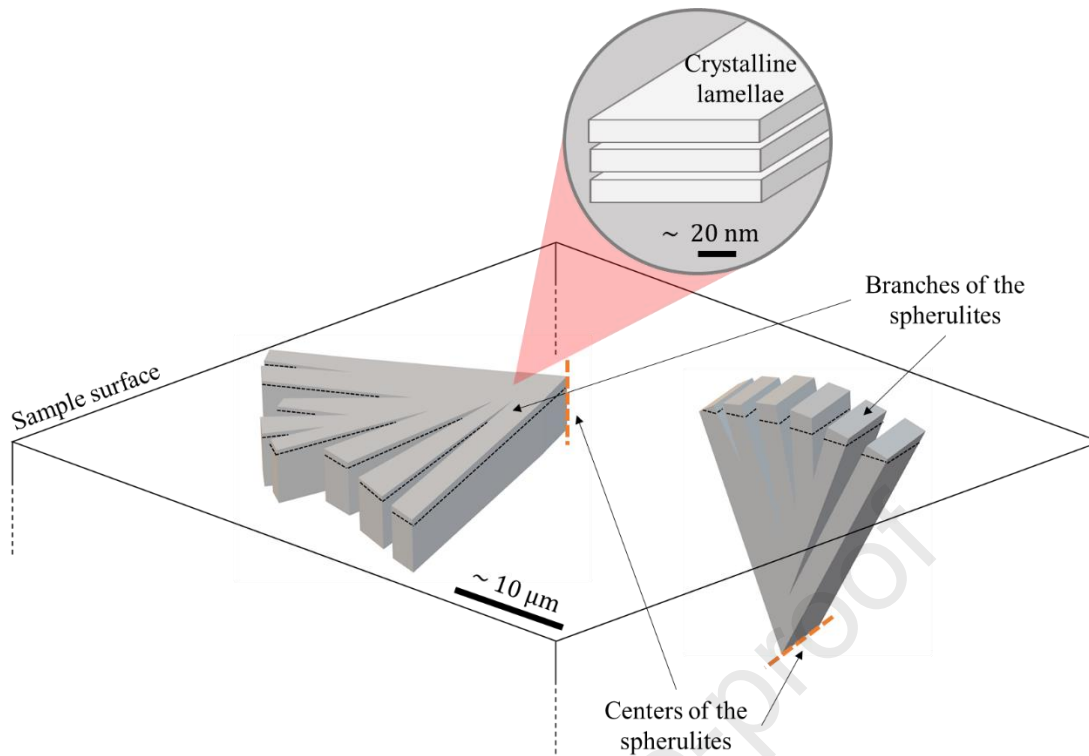
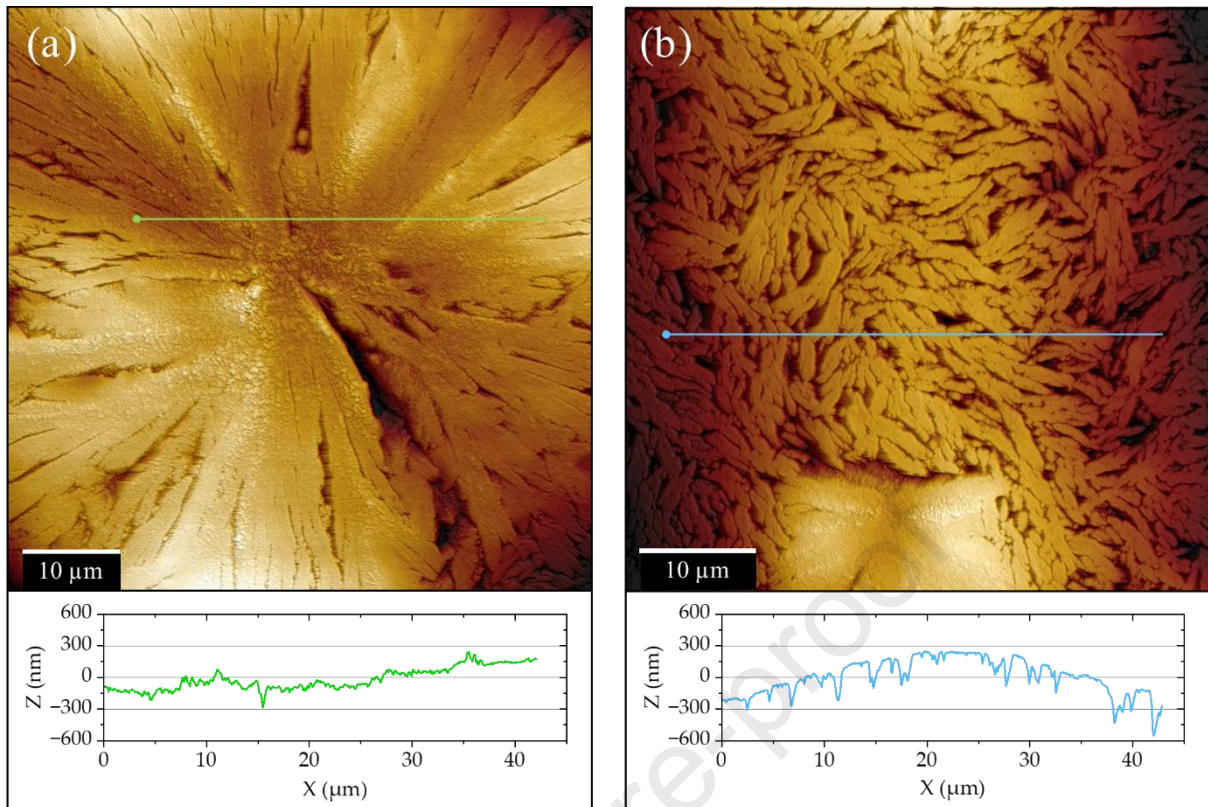


Fig. 4 - Schematic representation of surface-nucleated spherulite branches seen in a cross-section (left), and volume-nucleated spherulite branches seen in the periphery (right).

220

### 3.2 Characterization of the surface topography by AFM

The morphological complexity of the spherulites cannot be resolved by optical microscopy below the micron-level scale. Therefore, higher resolution techniques are required to observe  
 225 the intraspherulitic structure. In this study, complementary to optical microscopy, the AFM technique was used to provide 3D topography images with a lateral resolution at the nanometer scale. In addition, the AFM technique also provides information on surface roughness, which is crucial in our study as the nanoindentation technique requires a flat surface with a low level of roughness.



*Fig. 5 - AFM 3D top view topography images of the zones delimited by (a) the green square (labeled as 1) and (b) the blue square respectively on Fig. 2. The profile below corresponds to the indicated straight line.*

230

**Fig. 5.a** and **5.b** show respectively a (60×60 μm) and a (50×50 μm) AFM topography images represented in a 3D top view of the zones delimited by the green (labeled as 1) and the blue squares in **Fig. 3**. A profile has been added to provide quantitative topography information.

The spherulites nucleated near the surface (**Fig. 5.a**) present flat radial growth branches measuring 1-2 μm thick at their extremities, separated by cliffs up to 800 nm deep. Large flat regions are also present in their centers. The branches of the spherulites nucleated in the volume

235

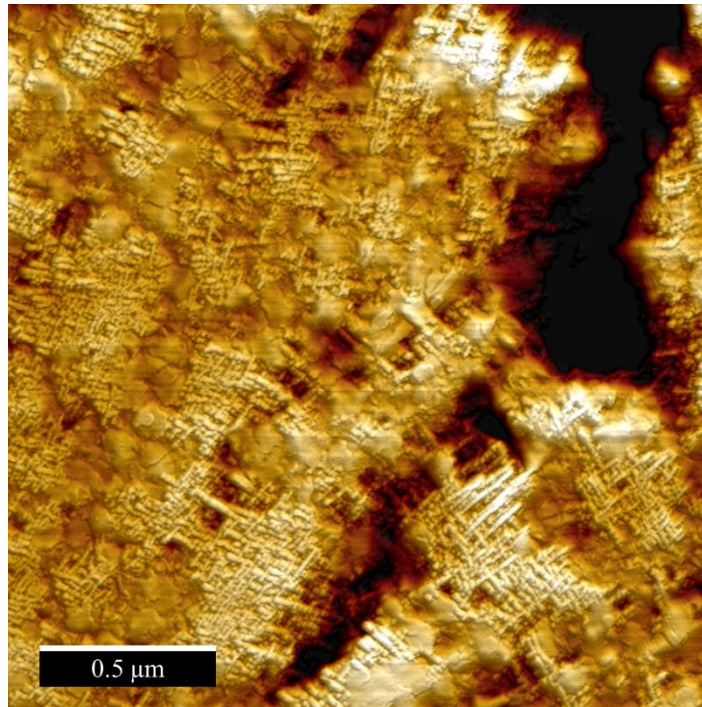


*Fig. 6 - AFM 3D top view scan of a zone on a surface-nucleated spherulite.*

(**Fig. 5.b**) present a width of 2-6 μm and are similar in thickness (1-2 μm) to surface-nucleated spherulites, with comparable cliffs. However, because the branching phenomenon is exacerbated at the extremity of the spherulite, the spherulites nucleated in the volume do not exhibit large flat regions unlike the spherulites nucleated near the surface.

The AFM technique allows measuring the RMS roughness (root mean square) of the surface,  $S_q$ , at the spherulite scale (large scale) and the branch scale (local scale). At the spherulite scale, the RMS roughness of the surface presented in **Fig. 5.a** and **Fig. 5.b**, are respectively  $S_{q_{\text{spherulite}}} = 164 \text{ nm}$  and  $S_{q_{\text{spherulite}}} = 236 \text{ nm}$ . These high values of roughness are explained by the presence of cliffs between the branches. As expected, the large-scale roughness is higher for the spherulites nucleated in the volume. However, for both surface- and volume-spherulites, the local roughness on the branches is much lower. Thus, taking the average roughness calculated on 10 areas of (2×2 μm) and (1.3×1.3 μm) respectively, distributed on the branches avoiding

the cliffs, the calculated roughness is  $Sq_{\text{branch}} = 16.0$  nm and  $Sq_{\text{branch}} = 14.1$  nm respectively.

250 This local roughness is directly related to the local organization of the crystalline lamellae.

The shiny areas seen under optical microscopy (**Fig. 3**) are not discernible from a topographic point of view. This shows that the brightness of these areas is not related to pollution of the surface, nor its topography, as one could be led to think by seeing the optical microscopy images but originates from a purely optical effect due to the specific nature of the material in this area, 255 or to a different microstructure buried below the surface.

At a nanometer scale, AFM scans also provide information on the complex lamellar organization of the microstructure. The crystalline lamellae, with a thickness of 15-20 nm, exhibit different orientations, and the characteristic cross-hatching phenomenon, typical of the  $\alpha$ -form spherulites of *i*-PP [42–45] is visible (**Fig. 6**). Thus, the presence of the  $\alpha$ -phase, as 260 suggested by the DSC and WAXS analyses, is confirmed by these observations.

### 3.3 Mechanical characterization of the surface

#### 3.3.1 Validity of the Measurements

265 The AFM measurements presented in the previous section revealed that the surface is not flat everywhere. However, the small roughness compared to the indentation depth and the flatness of the surface are important conditions to get reliable results from nanoindentation curves. To evaluate this reliability, the residual indents were observed firstly with optical microscopy and then with the AFM. The indents that fall into the cliffs of the surface were removed from the 270 analysis. The surface quality of the others was judged satisfactory from the AFM scans. An example of the topography of the indents on the spherulite 1 is presented in **Fig. 7. a, b**. Nine indents are visible and pointed at by white arrows on the large scan of  $15 \times 15$   $\mu\text{m}$  shown in **Fig**

275 **7.a.** These indents are from the first indentation grid with the step of 5  $\mu\text{m}$  between two adjacent ones. The observation reveals that the distance between neighboring indents is high enough to avoid any overlapping effect. Based on this observation, the distance between indents was reduced to 3  $\mu\text{m}$  for the following tests. It appears that the indents are well formed, with three symmetrical sides. This suggests that the surface is flat enough to correctly evaluate the value of the indentation modulus on these zones. Furthermore, no pile-up effect or cracks around the indents are observed which supports the validity of the mechanical properties obtained from the Oliver & Pharr method.

280 **Fig 7.b** presents a  $2 \times 2 \mu\text{m}$  scan of one of the indents observed in **Fig 7.a.** with a profile across the indent. The crystalline lamellae are distinguishable at both the image and the profile. They seem to be staked edge on and perpendicularly to the axis of the spherulite branch so that their thickness can be estimated at around 20 nm. The surface profile confirms that the indent is well-  
285 formed and that its depth is significant compared to the surface roughness. The corresponding force-displacement curve is presented in **Fig. 7.c.** One can notice that the depth of the indent measured by AFM is around 65 nm while the residual indentation depth on the corresponding indentation curve is 100 nm. This is due to the relaxation of the indents that continued after the nanoindentation measurements. Indeed, the presented AFM scan was acquired 20 days after the  
290 nanoindentation indent was formed.

To conclude this part, the residual indents have been carefully examined and selected based on the surface quality before being considered for the analysis that follows. The results presented in the next section are obtained only from the approved indents (a total of 62 indents were removed from the 583 indents, i.e. 10.6% of the total). The width of the residual indents is  
295 around 600 nm and their depth is around 65 nm. On this scale, the local arrangement of the lamellae is expected to have an impact on the mechanical properties of the tested volume.

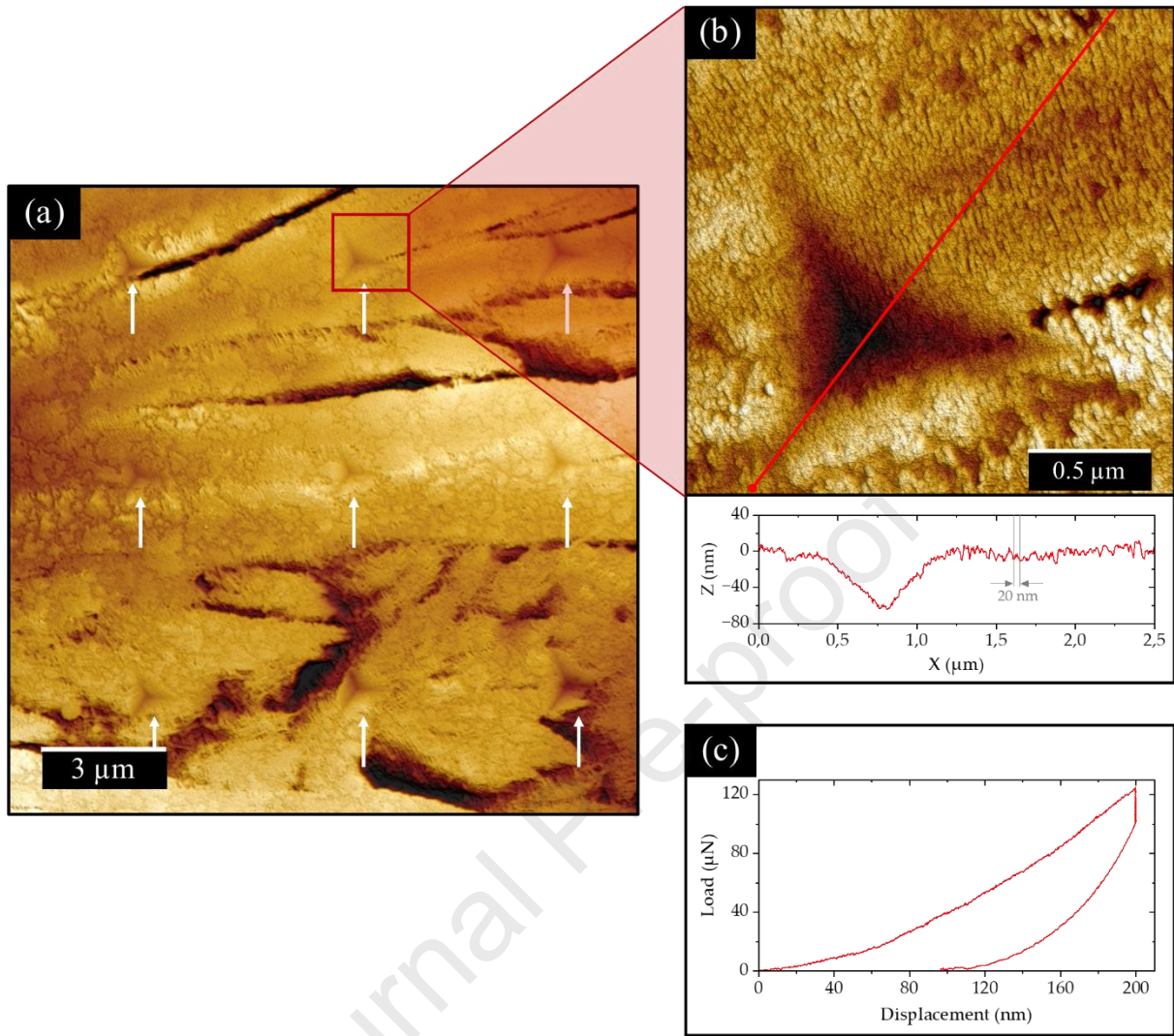


Fig. 7 – (a) AFM 3D top view scan of the indented surface of Spherulite A; (b) AFM 3D top view scan of an indent and profile of the red line; (c) Indentation curve of the corresponding indent.

## 3.3.2 Maps of elastic moduli of the spherulites

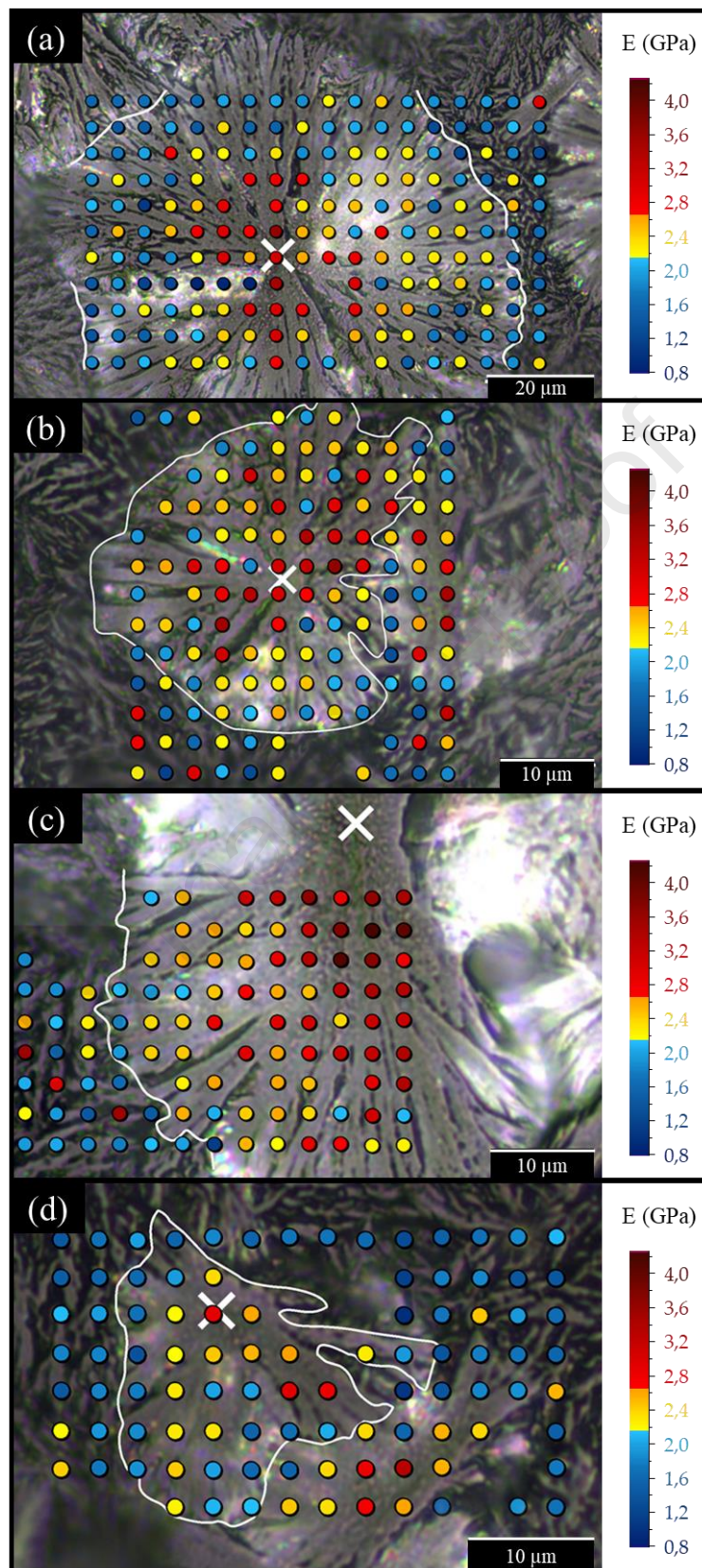


Fig. 8 - Indentation modulus mapping of the surface of four spherulites: (a) spherulite A, (b) spherulite B, (c) spherulite C and (d) spherulite D.

300 **Fig. 8** presents the elastic moduli obtained from the four indentation grids whose dimensions and protocol are presented in Section 2. In the following, the four spherulites contoured in each image are named spherulites A, B, C, and D for those presented in **Fig 8.a, 8.b, 8.c, and 8.d** respectively. These spherulites were chosen since all of them nucleated close to the surface, which permits the characterization of the heterogeneity of mechanical properties along the  
305 branches. The four present different stages of development associated with rather different shapes. Each grid covers not only the in-plane spherulite branches but also some surrounding spherulites with the branches edge on, growing from underneath the surface as schematized in **Fig. 4**. The indents of each array were observed by optical microscopy, and their positions were used to accurately superpose the elastic modulus value extracted from each indent on the optical  
310 microscopy image. Each point was assigned a color according to the value of the calculated indentation elastic modulus. White lines were drawn to delimit the edges of these spherulites.

The first observation from these results is that the elastic moduli obtained from the nanoindentation measurements over the four grids range between 0.8 and 4.2 GPa. The average value of all valid measurements is 2.22 GPa and the standard deviation is 0.56 GPa. This can  
315 be compared with Young's modulus of 1.8 GPa measured in a tensile test on a similar *i*-PP [46]. The observed differences can be attributed to variations in the considered measurement scale. Secondly, the maps in **Fig. 8.** present significant local variations of the elastic modulus on the surface. Since the quality of these measurements in relation to the surface roughness was approved in the previous section, all the differences in measured elastic moduli can be ascribed  
320 to the real difference in the mechanical response of the tested volume.

All four spherulites show an overall higher indentation modulus value in the central area (2.7 - 4.2 GPa), which then decreases progressively to the edges (1 - 2.2 GPa) through the transition

zones (2.2 - 2.7 GPa). The color scale on the maps was chosen to highlight these three zones within the spherulites. The elastic modulus values of the spherulite branches orthogonal to the surface are generally low ( $<2.2$  GPa).

As defined in Section 3.1, the indents from the four grids can be divided into two groups according to their location: those on the spherulites nucleated near the surface, which provide the mechanical properties all along the branches; and those on the spherulites nucleated in the volume, which characterize the mechanical behavior of the branches edge on, at their extremities. The results extracted from these two groups of indents will thus be analyzed separately in the following.

### 3.3.3 Distribution of elastic moduli in-plane along the spherulitic branches

Once the general tendencies are outlined, it is worth discussing the local elastic properties of each of the four spherulites in relation to their morphology. Spherulite A (**Fig. 8.a**) is the one in the green square in **Fig. 3**. It appears as quasi-circular, suggesting a well-advanced stage of growth. It is also the largest of the four, with an equivalent diameter (equivalent spherical representation) of  $d_{eq} = 83 \mu\text{m}$ . The second spherulite, spherulite B (**Fig. 8.b**), has a rosette-like shape with four lobes [42], and a growth obstructed by a neighboring smaller spherulite in its early stages (right), resulting in asymmetry. Its diameter is  $d_{eq} = 32 \mu\text{m}$ . The third spherulite, spherulite C (**Fig. 8.c**) presents a sheaf-like morphology with a clear principal growth direction from top to bottom of the picture. The indentation grid covers only this lower part of the spherulite. Finally, the fourth spherulite, spherulite D (**Fig. 8.d**), is the one that presents the least evolved stage of growth, limited to  $d_{eq} = 20 \mu\text{m}$  by the presence of an adjacent incipient

spherulite (right). The latter is also covered by the nanoindentation grid, but it is too small to be characterized with sufficient spatial resolution by nanoindentation.

Each tested spherulite presents a main diameter with a higher elastic modulus, as noticed through the red point alignments in **Fig. 8**. This effect is especially noticeable for spherulite C (Fig. 8.c). On the contrary, the shiny areas observed by optical microscopy and discussed in **Section 3.1** oriented perpendicularly from these diameters as well as the areas at the end of the spherulites branches have significantly lower elastic modulus values down to 0.8 GPa, as shown by the blue color in **Fig. 8**.

A possible explanation for this distribution of elastic moduli lies in density fluctuations related to spherulitic growth. Indeed, diameters of high elastic modulus values are correlated with the main growth axes of the spherulites. This characteristic sets them apart from the typical spherulite structure, as alpha *i*-PP spherulites exhibit two primary axes of growth [42]. Thus, these values can be attributed to a locally higher density of crystalline lamellae in those regions. On the other hand, the optical shiny areas correspond to the last stages of crystallization, before the material is completely cooled. In these regions, the local density of crystalline lamellae is much lower compared to the main growth axes, resulting in lower elastic modulus values.

Another possible explanation may be related to the local crystalline orientation within the spherulites. Indeed, it has been observed in the literature that during the spherulitic growth, the crystalline lamellae may be tilted with respect to the initial lamellae, especially in the regions on either side of the main growth axis where the spherulites close on themselves [47]. With the crystalline orientation being more coherent on the growth axes of the spherulites, the latter could present higher elastic modulus values. In contrast, the zones on both sides of these axes with a more disorganized crystalline orientation would present lower modulus values.

Since the elastic modulus is higher in the central zone and lower at the edges of all tested spherulites, it is interesting to examine its distribution as a function of the distance from the center. This is plotted and presented in **Fig. 9**. The centers of the spherulites were chosen on the optical images as the place where all the surface branches of the spherulite intersect. They are represented by a white cross in **Figs. 8 a-d**.

By plotting the variation of the modulus as a function of the distance to the center (**Fig. 9**), one can see clearly that there is a decrease in the indentation modulus with the distance from the center for all the tested spherulites. This result obtained by nanoindentation supports other results reported in the literature obtained by monotonic tension tests. Indeed, it has been shown qualitatively [15,19] and quantitatively [20] that the deformation at the edges of the spherulite was higher than at the center. This can be explained by the fact that the center of the spherulite, having developed first, presents a density of crystalline lamellae more important than the edges and thus higher elastic modulus values. Thus, the distance from the center appears to be a first-

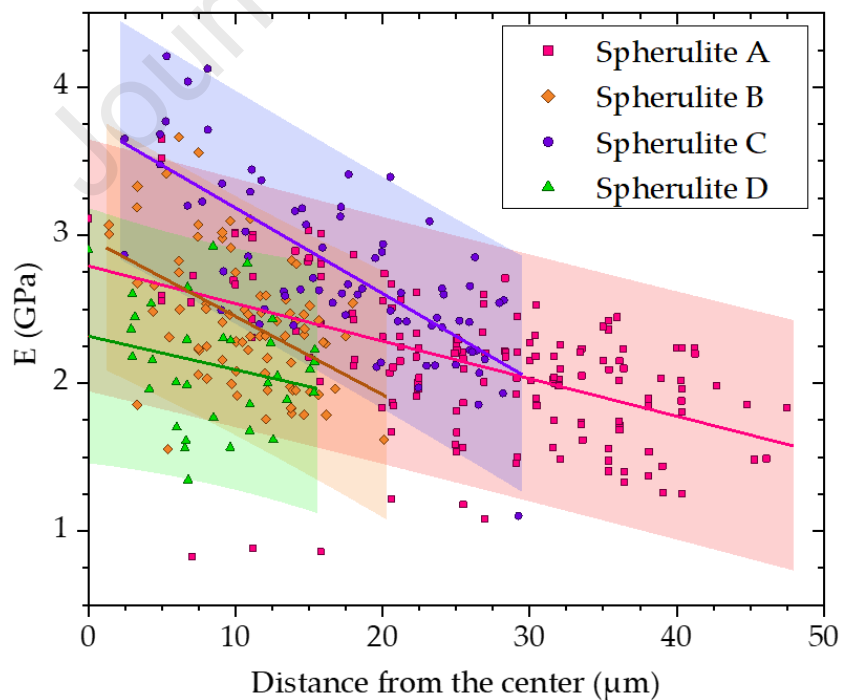


*Fig. 9 - Evolution of the indentation modulus as a function of the distance to the center of the surface-nucleated spherulites. A linear fit with 95% prediction bands is shown.*

order parameter on the value of the indentation modulus. The new data in **Fig. 9** show that the decrease of the modulus is linear and the slope ranges from  $-0.023$  to  $-0.058$  GPa/ $\mu\text{m}$  according to the spherulite considered. Despite the scattering of the results due to other factors discussed before and related to the anisotropic growth of the spherulite, the linear tendency is unquestionable.

Finally, the indentation modulus is similar at the edges of the four spherulites. By plotting a linear regression on the scatterplots in **Fig. 9** we obtain a mean value of indentation modulus on the edges of the same order of magnitude for the four spherulites  $E \sim 1.9$  GPa. Thus, the modulus values at the extremity of the branches do not depend on the size or position of the spherulite center.

### 3.3.4 Distribution of axially-measured elastic moduli at the ends of the spherulitic branches

395 This section will focus on the elastic moduli of the second group of measurements from the  
 grids presented in **Fig. 8**: the spherulites nucleated in the volume and tested in the axial direction  
 of the branches. **Fig. 10** shows the statistics of the indentation moduli obtained from these  
 indents (121 in total).

The average value of the indentation modulus is  $E = 1.91$  GPa with a standard deviation  $\sigma =$   
 400 0.46 GPa. This value is similar to the one measured at the end of the spherulite branches and  
 presented in the previous section. Thus, the mechanical properties are similar in both axial and  
 transverse directions of the spherulite branches close to their extremities. This result might seem  
 surprising since it is well known that single crystals, and in particular *i*-PP, do not exhibit  
 isotropic elastic properties [48]. However, one needs to consider the scale of the

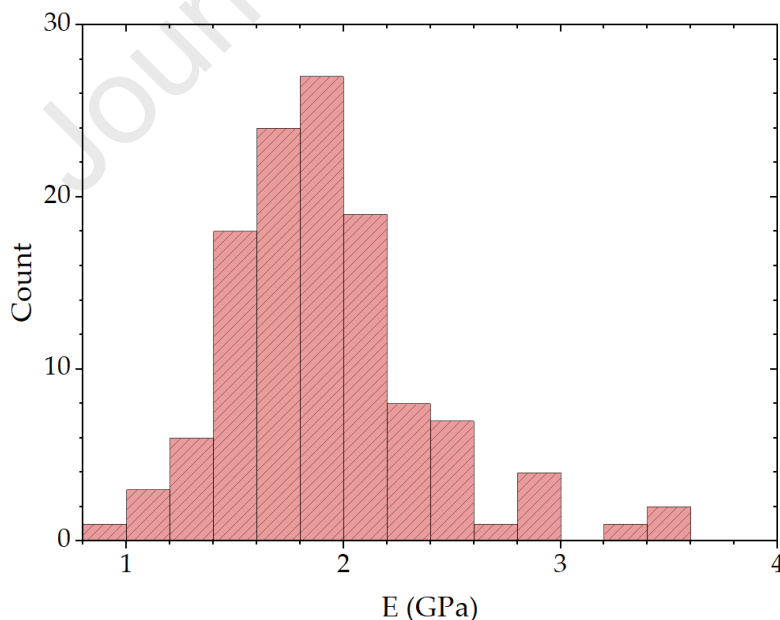


*Fig. 10 - Distribution of the elastic indentation moduli measured axially to the branches.*

405 nanoindentation test which covers many crystalline lamellae having different orientations in the tested volume. Therefore, the properties at this scale might very well be isotropic.

## 4 Conclusion

410 The use of nanoindentation enabled spatially resolved quantitative mechanical characterization at the intraspherulitic scale of an *i*-PP semi-crystalline polymer. Several results from the nanoindentation mappings can be highlighted.

(i) It was shown experimentally that there is a decreasing gradient of elastic modulus from the center of the spherulites to the edges. The higher elastic modulus observed in the center of the spherulite can be attributed to its higher density of crystalline lamellae compared to the edges.

415 (ii) Furthermore, the main growth axes of the spherulites have the highest modulus values, while the regions on either side of these axes present a lower elastic modulus. This again can be related to a lower lamellar density or a different or less ordered orientation of the lamellae in the stack.

420 (iii) Finally, at the scales tested, the end of the branches of spherulites has similar mechanical properties in the transverse and longitudinal directions with respect to their growth axis. A volume of nanoindentation test sufficient to include many crystalline lamellae with different orientations and thus masking local anisotropy can explain this result.

425 The nanoindentation results were completed by AFM observations of the tested spherulites. It has thus been shown that the probed volumes were of the same order of magnitude as a bundle of crystalline lamellae. Finally, this study shed new insight into the scale transition in the

context of semi-crystalline materials by providing quantitative values of the mechanical properties at the intraspherulitic scale and by making clear links with the microstructure.

430 To deepen our understanding of the mechanical behavior of semi-crystalline polymers, it is possible to extend this study to the finer scale of crystalline lamellae using AFM mechanical testing. This technique would enable probing the local scale of crystalline lamellae and refine the spatial resolution of intraspherulitic mechanical heterogeneities. This outlook opens exciting prospects for future research, as it may elucidate further subtleties in the mechanical  
435 behavior of semi-crystalline materials.

## Acknowledgments

The authors thank Prof. Pierre Olivier Renault for his experimental support for the X-Ray  
440 analysis, and Prof. Bernard Lotz for fruitful discussions. Institut Pprime gratefully acknowledges "Contrat de Plan Etat - Région Nouvelle-Aquitaine" (CPER) as well as the "Fonds Européen de Développement Régional" (FEDER) [reference n°2017-3528710 (MAMMOUTH)] for their financial support to the reported work. This work pertains to the French Government programs "Investissements d'Avenir" LABEX INTERACTIFS [reference  
445 ANR-11-LABX-0017-01] and EUR INTREE [reference ANR-18-EURE-0010]. ISAE-ENSMA is acknowledged for the grant of a doctoral fellowship to J. Grondin.

## References

- 450 [1] J. Patel, P.J. Phillips, The young's modulus of polyethylene, *Journal of Polymer Science: Polymer Letters Edition*. 11 (1973) 771–776. <https://doi.org/10.1002/pol.1973.130111208>.
- [2] B. Crist, C.J. Fisher, P.R. Howard, Mechanical properties of model polyethylenes: tensile elastic modulus and yield stress, *Macromolecules*. 22 (1989) 1709–1718. <https://doi.org/10.1021/ma00194a035>.
- 455 [3] X. Lu, R. Qian, N. Brown, The effect of crystallinity on fracture and yielding of polyethylenes, *Polymer*. 36 (1995) 4239–4244. [https://doi.org/10.1016/0032-3861\(95\)92219-5](https://doi.org/10.1016/0032-3861(95)92219-5).
- [4] N.W. Brooks, M. Ghazali, R.A. Duckett, A.P. Unwin, I.M. Ward, Effects of morphology on the yield stress of polyethylene, *Polymer*. 40 (1999) 821–825. [https://doi.org/10.1016/S0032-3861\(98\)00324-3](https://doi.org/10.1016/S0032-3861(98)00324-3).
- 460 [5] R.J. Davies, N.E. Zafeiropoulos, K. Schneider, S.V. Roth, M. Burghammer, C. Riekel, J.C. Kotek, M. Stamm, The use of synchrotron X-ray scattering coupled with in situ mechanical testing for studying deformation and structural change in isotactic polypropylene, *Colloid Polym Sci*. 282 (2004) 854–866. <https://doi.org/10.1007/s00396-004-1118-z>.
- [6] A. Pawlak, A. Galeski, Cavitation and morphological changes in polypropylene deformed at elevated temperatures, *Journal of Polymer Science Part B: Polymer Physics*. 48 (2010) 1271–1280. <https://doi.org/10.1002/polb.22020>.
- 465 [7] S. Humbert, O. Lame, R. Séguéla, G. Vigier, A re-examination of the elastic modulus dependence on crystallinity in semi-crystalline polymers, *Polymer*. 52 (2011) 4899–4909. <https://doi.org/10.1016/j.polymer.2011.07.060>.
- 470 [8] C. Millot, R. Séguéla, O. Lame, L.-A. Fillot, C. Rochas, P. Sotta, Tensile Deformation of Bulk Polyamide 6 in the Preyield Strain Range. Micro–Macro Strain Relationships via in Situ SAXS and WAXS, *Macromolecules*. 50 (2017) 1541–1553. <https://doi.org/10.1021/acs.macromol.6b02471>.
- [9] H. Guo, R.G. Rinaldi, S. Tayakout, M. Broudin, O. Lame, The correlation between the mixed-mode oligo-cyclic loading induced mechanical and microstructure changes in HDPE, *Polymer*. 224 (2021) 123706. <https://doi.org/10.1016/j.polymer.2021.123706>.
- 475 [10] A. Voss, R.W. Stark, C. Dietz, Surface versus Volume Properties on the Nanoscale: Elastomeric Polypropylene, *Macromolecules*. 47 (2014) 5236–5245. <https://doi.org/10.1021/ma500578e>.
- [11] X. Wu, S. Shi, Z. Yu, T.P. Russell, D. Wang, AFM nanomechanical mapping and nanothermal analysis reveal enhanced crystallization at the surface of a semicrystalline polymer, *Polymer*. 146 (2018) 188–195. <https://doi.org/10.1016/j.polymer.2018.05.043>.
- 480 [12] M. Mousa, Y. Dong, 5 - A critical role of interphase properties and features on mechanical properties of poly(vinyl alcohol) (PVA) bionanocomposites: nanoscaled characterisation and modelling, in: K.L. Goh, A. M.k., R.T. De Silva, S. Thomas (Eds.), *Interfaces in Particle and Fibre Reinforced Composites*, Woodhead Publishing, 2020: pp. 115–136. <https://doi.org/10.1016/B978-0-08-102665-6.00005-4>.
- 485 [13] V. Ferreiro, Y. Pennec, R. Séguéla, G. Coulon, Shear banding in polyamide 6 films as revealed by atomic force microscopy, *Polymer*. 41 (2000) 1561–1569. [https://doi.org/10.1016/S0032-3861\(99\)00276-1](https://doi.org/10.1016/S0032-3861(99)00276-1).
- [14] V. Ferreiro, G. Coulon, Shear banding in strained semicrystalline polyamide 6 films as revealed by atomic force microscopy: Role of the amorphous phase, *Journal of Polymer Science Part B: Polymer Physics*. 42 (2004) 687–701. <https://doi.org/10.1002/polb.10731>.
- 490 [15] C. Thomas, V. Ferreiro, G. Coulon, R. Seguela, In situ AFM investigation of crazing in polybutene spherulites under tensile drawing, *Polymer*. 48 (2007) 6041–6048. <https://doi.org/10.1016/j.polymer.2007.07.062>.
- 495 [16] F. Detrez, S. Cantournet, R. Seguela, Plasticity/damage coupling in semi-crystalline polymers prior to yielding: Micromechanisms and damage law identification, *Polymer*. 52 (2011) 1998–2008. <https://doi.org/10.1016/j.polymer.2011.03.012>.
- [17] I. Raphael, N. Saintier, G. Robert, J. Béga, L. Laiarinandrasana, On the role of the spherulitic microstructure in fatigue damage of pure polymer and glass-fiber reinforced semi-crystalline polyamide 6.6, *International Journal of Fatigue*. 126 (2019) 44–54. <https://doi.org/10.1016/j.ijfatigue.2019.04.036>.
- 500

- [18] N. Selles, P. Cloetens, H. Proudhon, T.F. Morgenev, O. Klinkova, N. Saintier, L. Laiarinandrasana, Voiding Mechanisms in Deformed Polyamide 6 Observed at the Nanometric Scale, *Macromolecules*. 50 (2017) 4372–4383. <https://doi.org/10.1021/acs.macromol.7b00727>.
- 505 [19] L. Laiarinandrasana, N. Selles, O. Klinkova, T. Morgenev, H. Proudhon, L. Helfen, Structural versus microstructural evolution of semi-crystalline polymers during necking under tension: Influence of the skin-core effects, the relative humidity and the strain rate, (2016). <https://doi.org/10.1016/J.POLYMERTESTING.2016.09.012>.
- [20] J.M. Teixeira Pinto, F. Touchard, S. Castagnet, C. Nadot-Martin, D. Mellier, DIC Strain Measurements at the Micro-Scale in a Semi-Crystalline Polymer, *Exp Mech*. 53 (2013) 1311–1321. <https://doi.org/10.1007/s11340-013-9753-2>.
- 510 [21] B. Crist, J.M. Schultz, Polymer spherulites: A critical review, *Progress in Polymer Science*. 56 (2016) 1–63. <https://doi.org/10.1016/j.progpolymsci.2015.11.006>.
- [22] G.Z. Voyiadjis, L. Malekmoie, A. Samadi-Dooki, Indentation size effect in amorphous polymers based on shear transformation mediated plasticity, *Polymer*. 137 (2018) 72–81. <https://doi.org/10.1016/j.polymer.2018.01.006>.
- 515 [23] P. Christöfl, C. Czibula, M. Berer, G. Oreski, C. Teichert, G. Pinter, Comprehensive investigation of the viscoelastic properties of PMMA by nanoindentation, *Polymer Testing*. 93 (2021) 106978. <https://doi.org/10.1016/j.polymertesting.2020.106978>.
- 520 [24] P.-E. Mazeran, M. Beyaoui, M. Bigerelle, M. Guigon, Determination of mechanical properties by nanoindentation in the case of viscous materials, *International Journal of Materials Research*. 103 (2012) 715–722. <https://doi.org/10.3139/146.110687>.
- [25] O. Smerdova, M. Pecora, M. Gigliotti, Cyclic indentation of polymers: Instantaneous elastic modulus from reloading, energy analysis, and cyclic creep, *Journal of Materials Research*. (2019) 1–11. <https://doi.org/10.1557/jmr.2019.289>.
- 525 [26] G. Hochstetter, A. Jimenez, J.L. Loubet, Strain-rate effects on hardness of glassy polymers in the nanoscale range. Comparison between quasi-static and continuous stiffness measurements, *Journal of Macromolecular Science, Part B*. 38 (1999) 681–692. <https://doi.org/10.1080/00222349908248131>.
- 530 [27] P. Christöfl, C. Czibula, T. Seidlhofer, M. Berer, A. Macher, E. Helfer, T. Schrank, G. Oreski, C. Teichert, G. Pinter, Morphological characterization of semi-crystalline POM using nanoindentation, *International Journal of Polymer Analysis and Characterization*. 26 (2021) 692–706. <https://doi.org/10.1080/1023666X.2021.1968122>.
- [28] R. Lesan-Khosh, R. Bagheri, S. Asgari, Nanoindentation of isotactic polypropylene: Correlations between hardness, yield stress, and modulus on the local and global scales, *Journal of Applied Polymer Science*. 121 (2011) 930–938. <https://doi.org/10.1002/app.33635>.
- 535 [29] S. Liparoti, A. Sorrentino, V. Speranza, G. Titomanlio, Multiscale mechanical characterization of iPP injection molded samples, *European Polymer Journal*. 90 (2017) 79–91. <https://doi.org/10.1016/j.eurpolymj.2017.03.010>.
- 540 [30] S. Liparoti, A. Sorrentino, V. Speranza, Morphology-Mechanical Performance Relationship at the Micrometrical Level within Molded Polypropylene Obtained with Non-Symmetric Mold Temperature Conditioning, *Polymers*. 13 (2021) 462. <https://doi.org/10.3390/polym13030462>.
- [31] T. Iqbal, B.J. Briscoe, S. Yasin, P.F. Luckham, Nanoindentation response of poly(ether ether ketone) surfaces—A semicrystalline bimodal behavior, *Journal of Applied Polymer Science*. 130 (2013) 4401–4409. <https://doi.org/10.1002/app.39723>.
- 545 [32] T. Iqbal, S.S. Camargo, S. Yasin, U. Farooq, A. Shakeel, Nano-Indentation Response of Ultrahigh Molecular Weight Polyethylene (UHMWPE): A Detailed Analysis, *Polymers*. 12 (2020) 795. <https://doi.org/10.3390/polym12040795>.
- [33] G.Z. Voyiadjis, A. Samadi-Dooki, L. Malekmoie, Nanoindentation of high performance semicrystalline polymers: A case study on PEEK, *Polymer Testing*. 61 (2017) 57–64. <https://doi.org/10.1016/j.polymertesting.2017.05.005>.
- 550 [34] T. Labour, L. Ferry, C. Gauthier, P. Hajji, G. Vigier,  $\alpha$ - and  $\beta$ -crystalline forms of isotactic polypropylene investigated by nanoindentation, *Journal of Applied Polymer Science*. 74 (1999) 195–200. [https://doi.org/10.1002/\(SICI\)1097-4628\(19991003\)74:1<195::AID-APP24>3.0.CO;2-8](https://doi.org/10.1002/(SICI)1097-4628(19991003)74:1<195::AID-APP24>3.0.CO;2-8).
- 555 8.

- [35] P. Enrique-Jimenez, J. Vega, J. Martínez-Salazar, F. Ania, A. Flores, Mapping the Mechanical Properties of Poly(3-hydroxybutyrate-co-3-hydroxyvalerate) Banded Spherulites by Nanoindentation, *Polymers*. 8 (2016) 358. <https://doi.org/10.3390/polym8100358>.
- 560 [36] F. Bédoui, F. Sansoz, N.S. Murthy, Incidence of nanoscale heterogeneity on the nanoindentation of a semicrystalline polymer: Experiments and modeling, *Acta Materialia*. 56 (2008) 2296–2306. <https://doi.org/10.1016/j.actamat.2008.01.021>.
- [37] D. Hoffman, I. Miskioglu, K.E. Aifantis, J. Drelich, Measuring the Surface and Bulk Modulus of Polished Polymers with AFM and Nanoindentation, *Journal of Adhesion Science and Technology*. 26 (2012) 1201–1220. <https://doi.org/10.1163/156856111X593540>.
- 565 [38] J. Varga, Supermolecular structure of isotactic polypropylene, *J Mater Sci*. 27 (1992) 2557–2579. <https://doi.org/10.1007/BF00540671>.
- [39] B. Monasse, J.M. Haudin, Growth transition and morphology change in polypropylene, *Colloid & Polymer Sci*. 263 (1985) 822–831. <https://doi.org/10.1007/BF01412960>.
- 570 [40] W.C. Oliver, G.M. Pharr, An improved technique for determining hardness and elastic modulus using load and displacement sensing indentation experiments, *Journal of Materials Research*. 7 (1992) 1564–1583. <https://doi.org/10.1557/JMR.1992.1564>.
- [41] R.J. Crawford, CHAPTER 2 - Mechanical Behaviour of Plastics, in: R.J. Crawford (Ed.), *Plastics Engineering (Third Edition)*, Butterworth-Heinemann, Oxford, 1998: pp. 41–167. <https://doi.org/10.1016/B978-075063764-0/50004-2>.
- 575 [42] R.H. Olley, D.C. Bassett, On the development of polypropylene spherulites, *Polymer*. 30 (1989) 399–409. [https://doi.org/10.1016/0032-3861\(89\)90004-9](https://doi.org/10.1016/0032-3861(89)90004-9).
- [43] F. Khoury, The spherulitic crystallization of isotactic polypropylene from solution: On the evolution of monoclinic spherulites from dendritic chain-folded crystal precursors, *J. RES. NATL. BUR. STAN. SECT. A*. 70A (1966) 29. <https://doi.org/10.6028/jres.070A.006>.
- 580 [44] B. Lotz, J.C. Wittmann, The molecular origin of lamellar branching in the  $\alpha$  (monoclinic) form of isotactic polypropylene, *Journal of Polymer Science Part B: Polymer Physics*. 24 (1986) 1541–1558. <https://doi.org/10.1002/polb.1986.090240712>.
- [45] J.-J. Zhou, J.-G. Liu, S.-K. Yan, J.-Y. Dong, L. Li, C.-M. Chan, J.M. Schultz, Atomic force microscopy study of the lamellar growth of isotactic polypropylene, *Polymer*. 46 (2005) 4077–4087. <https://doi.org/10.1016/j.polymer.2005.03.047>.
- 585 [46] D. Vgenopoulos, J. Sweeney, C.A. Grant, G.P. Thompson, P.E. Spencer, P. Caton-Rose, P.D. Coates, Nanoindentation analysis of oriented polypropylene: Influence of elastic properties in tension and compression, *Polymer*. 151 (2018) 197–207. <https://doi.org/10.1016/j.polymer.2018.07.080>.
- 590 [47] L.G.M. Beekmans, G.J. Vancso, Real-time crystallization study of poly( $\epsilon$ -caprolactone) by hot-stage atomic force microscopy, *Polymer*. 41 (2000) 8975–8981. [https://doi.org/10.1016/S0032-3861\(00\)00240-8](https://doi.org/10.1016/S0032-3861(00)00240-8).
- [48] D.H. Chung, W.R. Buessem, The Elastic Anisotropy of Crystals, *Journal of Applied Physics*. 38 (1967) 2010–2012. <https://doi.org/10.1063/1.1709819>.
- 595

Highlights

# **Intraspherulitic mechanical heterogeneities and microstructure of *i*-PP highlighted by Nanoindentation and Atomic Force Microscopy**

Jérémy GRONDIN\*<sup>1</sup>, Olga SMERDOVA<sup>1</sup>, Sylvie CASTAGNET<sup>1</sup>, Christophe TROMAS<sup>1</sup>

<sup>1</sup>Institut Pprime (UPR 3346 CNRS / ISAE-ENSMA / UNIVERSITÉ DE POITIERS), Department of Physics and Mechanics of Materials, 1 Avenue Clement Ader, BP 40109, Futuroscope, 86961, Cedex, France

\*Corresponding author.

Email address: [jeremy.grondin@ensma.fr](mailto:jeremy.grondin@ensma.fr) (J. Grondin)

- Mapping of elastic modulus in *i*-PP bulk spherulites using nanoindentation.
- Spherulitic micro- and nanostructure characterized by Atomic Force Microscopy.
- Spherulite center is stiffer than its edges.
- Mechanical properties depend on growth stage and lamellae organization.

**Declaration of interests**

The authors declare that they have no known competing financial interests or personal relationships that could have appeared to influence the work reported in this paper.

The authors declare the following financial interests/personal relationships which may be considered as potential competing interests:

Journal Pre-proof